Diffusiophoresis of two-dimensional liquid droplets in a phase-separating system

Natalia Vladimirova,[1] Andrea Malagoli,[2] and Roberto Mauri[1]
[1]*Department of Chemical Engineering, The City College of CUNY, New York, New York 10031*
[2]*Department of Astronomy and Astrophysics, University of Chicago, Chicago, Illinois 60637*
(Received 4 September 1998)

The motion of phase-separating liquid drops was simulated in two dimensions following the model *H*, where convection and diffusion are coupled via a body force, expressing the tendency of demixing systems to minimize their free energy. This driving force depends on the capillary number, i.e., the ratio of viscous to thermal forces, which in a typical case is of order 10^{-4}, inducing a convective material flux much larger than its diffusive counterpart. Three problems were considered. In the first, we studied the motion of a single drop immersed in a continuum field with constant concentration gradient, finding that the drop speed is proportional to the concentration gradient and inversely proportional to the capillary number. In the second problem, we found that the motion of a single drop immersed in a homogeneous concentration field depends on the difference $(\Delta\phi)_0$ between the initial concentration of the continuum phase and its equilibrium value. In fact, when $(\Delta\phi)_0<0$, the drop shrinks without moving, while when $(\Delta\phi)_0>0$, the drop consumes material from the surrounding field and moves randomly, propelled by the induced capillary driving force. During its movement, the drop grows linearly in time, with a growth rate proportional to the ratio between molecular diffusivity and interface thickness. In addition, during its random motion, the drop mean square displacement grows linearly with time, with an effective diffusion coefficient which is of the same magnitude as the molecular diffusivity. The predicted drop growth rate and mean velocity are in good agreement with experimental observations. Finally, the motion of two drops is studied, showing that the capillary forces induce a mutual attraction between the two drops. When $(\Delta\phi)_0<0$, the attractive force is unchallenged, thus leading always to coalescence, while when $(\Delta\phi)_0>0$ a screening effect arises which may keep the two drops apart from each other. [S1063-651X(99)10108-9]

PACS number(s): 64.70.Ja, 68.35.Rh. 68.10.−m, 68.35.Fx

I. INTRODUCTION

In a series of experimental studies [1] it has been observed that, during the phase separation of deeply quenched liquid mixures having waterlike viscosity, 50 micron-size drops grow at a rate of ~ 100 μm/s and move at speeds exceeding 200 μm/s, indicating that the process is driven by convection, and not by diffusion. In this work, we intend to model this experimentally observed rapid movement of phase separating liquid drops, determining the driving force that is responsible for it.

Most of the previous studies on phase separation [2–4] have considered systems near their miscibility curve, observing that, right after the temperature has crossed that of the miscibility curve, the system starts to separate by diffusion only, leading to the formation of well-defined patches, whose average concentration is not too far from its equilibrium value. The shape of these patches appears to depend strongly on the composition of the system: for critical mixtures, they are dendritic, bicontinuous domains, while for off-critical systems they appear to be spherical drops. Then, in the so called, ''late'' stage of coarsening, these patches grow by diffusion and coalescence, until they become large enough that buoyancy dominates surface tension effects, and the mixture separates by gravity. This occurs when the size of the domains is $\ell_{\max}=O(\sigma/g\Delta\rho)$, where σ is the surface tension, g the gravity field, and $\Delta\rho$ the density difference between the two separating phases [5]. So, during the process of phase separation, the morphology of the system changes dramatically from that of an unstructured fluid to that of an emulsion, with the phase interfaces being initially nonexisting, then very diffuse and, finally, rather sharp [6].

In this work, the evolution of critical binary mixtures is studied, assuming that, initially, the system is composed of small drops, separated from the continuum phase by sharp interfaces. At this point, instead of tracking down the movement of these interfaces, we assume that the mole fraction, ϕ, and the mean velocity, $\mathbf{v}$, of the mixture are continuous functions of the position, solving the equations of conservation of mass and momentum. According to the so-called model *H* [7], following the classification by Hohenberg and Halperin [8], transport of mass and momentum are coupled to each other via a composition-dependent body force $\mathbf{F}_\phi$ which incorporates capillary effects. In fact, as noted by Jasnow and Viñals [9], when the system is composed of single-phase domains separated by sharp interfaces, $\mathbf{F}_\phi$ reduces to a Marangoni force. This body force is responsible for the strong motion of the single-phase domains that is observed experimentally during phase transition [1]. In particular, as noted by Karpov [10] and Karpov and Oxtoby [11], capillary forces drive the motion of nucleating droplets along a composition gradient, leading to particle clustering and direct coalescence. These aspects of the phenomenon of phase separation are further studied here.

The approach that is used in this work can be extended to study many multiphase systems. In fact, multiphase flows can be simulated in two ways, assuming that the different phases are either separated by a sharp surface of discontinuity or merge gradually into one another. In the first approach, the governing equations are solved in each phase, subjected

to boundary conditions at the interfaces, which, in turn, have to be tracked down as they move. In the second approach, we assume that the two phases are coexisting at each point, and that, even when two separate single-phase regions can be identified, the interface between them is diffuse. The first, moving boundary scheme is preferable when the two phases are immiscible with each other, so that the interface width, set by the range of the intermolecular forces, is much smaller than the typical length scale of the fluid flow. On the other hand, the second, diffuse interface approach applies when the two phases are miscible with each other, so that the width of the transition region is comparable to the typical lengthscale of the fluid flow. In this work, we study the motion of partially miscible fluid mixtures using the diffuse interface approach, although, at least in principle, either of the two schemes is applicable and, actually, the moving boundary approach is more widely used.

After revisiting in Sec. II the governing equations, in Sec. III we consider three examples of diffusiophoresis of drops in two dimensions, that is their motion induced by the concentration gradients of the background field. First, we study the motion of a single drop immersed in a constant concentration gradient of the continuum phase; then, we follow its motion as it phase separates in a uniform background field; finally, the influence of the capillary body force on the coalescence rate of drops is analyzed, simulating the motion of two drops and studying the resulting mutual attractive force.

II. THE GOVERNING EQUATIONS

The motion of an incompressible binary fluid mixture composed of two species A and B is described through the so-called model H [8]. Here, A and B are assumed to have equal viscosities, densities, and molecular weights, with the composition of the system uniquely determined through the molar fraction ϕ of, say, species A.

If the flow is assumed to be slow enough to neglect the dynamic terms in the Navier-Stokes equation, conservations of mass and momentum lead to the following system of equation:

$$\frac{\partial \phi}{\partial t}+\mathbf{v}\cdot\boldsymbol{\nabla}\phi=-\frac{1}{\rho}\boldsymbol{\nabla}\cdot\mathbf{j}, \tag{1}$$

$$\eta\nabla^2\mathbf{v}-\boldsymbol{\nabla}p=-\mathbf{F}_\phi, \tag{2}$$

$$\boldsymbol{\nabla}\cdot\mathbf{v}=0, \tag{3}$$

where $\mathbf{v}$ is the average local fluid velocity, $\mathbf{j}$ is the diffusion flux [12], and $\mathbf{F}_\phi$ is a body force. As shown in previous works [13], $\mathbf{j}$ is determined through the relation

$$\mathbf{j}=-\rho\phi(1-\phi)D\boldsymbol{\nabla}\mu, \tag{4}$$

where ρ is the density of the system, D the temperature-dependent diffusion coefficient, and $\mu=\mu_A-\mu_B$ the generalized chemical potential defined as [12]

$$\mu=\frac{\delta(G/RT)}{\delta\phi}, \tag{5}$$

with G denoting the molar Gibbs free energy, averaged over a small volume $\mathcal{V}$ of the system,

$$G=\frac{1}{\mathcal{V}}\int g\,d\mathbf{r}. \tag{6}$$

Here g denotes the generalized specific free energy [14,13,9],

$$g=g_A\phi+g_B(1-\phi)+RT[\phi\ln\phi+(1-\phi)\ln(1-\phi)]$$
$$+RT\Psi\phi(1-\phi)+\frac{1}{2}RTa^2(\boldsymbol{\nabla}\phi)^2, \tag{7}$$

where g_A and g_B are the molar free energies of the pure species A and B, respectively, at temperature T and pressure p, R is the gas constant, Ψ the Flory parameter, and a is a characteristic microscopic length. As shown by Van der Waals [15], the characteristic length a is proportional to the surface tension at equilibrium σ, as σ is the energy stored in the unit interfacial area at equilibrium, i.e.,

$$\sigma=\frac{1}{2}\frac{\rho RT}{M_W}a^2\int(\boldsymbol{\nabla}\phi)^2\,dx\approx\frac{\rho RT}{M_W}a\sqrt{\Psi-2}(\Delta\phi)_{\mathrm{eq}}^2, \tag{8}$$

where $(\Delta\phi)_{\mathrm{eq}}$ is the composition difference between the two phases at equilibrium, while M_W is the molecular weight of species A and B, and we have considered that the thickness of the interface is $\ell\approx a/\sqrt{\Psi-2}$ [13]. Considering that $(\Delta\phi)_{\mathrm{eq}}\sim\sqrt{\Psi-2}$, we obtain

$$a\sim(\Psi-2)^{-3/2}\frac{\sigma M_W}{\rho RT}. \tag{9}$$

The body force $\mathbf{F}_\phi$ appearing in Eq. (2) equals the gradient of the free energy [8], and therefore it is driven by the concentration gradients within the mixture [16,9]

$$\mathbf{F}_\phi=\frac{\rho}{M_W}\boldsymbol{\nabla}g=\left(\frac{\rho RT}{M_W}\right)\mu\boldsymbol{\nabla}\phi. \tag{10}$$

This force, being proportional to $\mu=\mu_A-\mu_B$, is driven by the surface energy, and therefore can be interpreted as a capillary force. Physically, $\mathbf{F}_\phi$ tends to minimize the energy stored at the interface, driving, say, A-rich drops towards A-rich region, and therefore enhancing coalescence.

Now, we restrict our analysis to two dimensional systems, so that the velocity $\mathbf{v}$ can be expressed in terms of a stream function ψ, i.e.,

$$v_1=\partial\psi/\partial r_2,\quad v_2=-\partial\psi/\partial r_1. \tag{11}$$

Consequently, substituting Eq. (11) into Eqs. (1)–(3), we obtain

$$\frac{\partial\phi}{\partial t}=\boldsymbol{\nabla}\psi\times\boldsymbol{\nabla}\phi-\frac{1}{\rho}\boldsymbol{\nabla}\cdot\mathbf{j}, \tag{12}$$

$$\eta\nabla^4\psi=\left(\frac{\rho RT}{M_W}\right)\boldsymbol{\nabla}\mu\times\boldsymbol{\nabla}\phi, \tag{13}$$

where

$$\mathbf{A}\times\mathbf{B}=A_1B_2-A_2B_1.$$

Since the main mechanism of mass transport at the beginning of the phase segregation is diffusion, the length scale of the process is the microscopic length a. Therefore, using the scaling

$$\tilde{r}=\frac{1}{a}r, \quad \tilde{t}=\frac{D}{a^2}t, \quad \tilde{\psi}=\frac{\mathrm{Ca}}{D}\psi, \tag{14}$$

we obtain

$$\frac{\partial\phi}{\partial\tilde{t}}=\mathrm{Ca}^{-1}\tilde{\nabla}\tilde{\psi}\times\tilde{\nabla}\phi+\tilde{\nabla}\cdot(\tilde{\nabla}\phi-\phi(1-\phi)[2\Psi+\tilde{\nabla}^2]\tilde{\nabla}\phi), \tag{15}$$

$$\tilde{\nabla}^4\tilde{\psi}=-\tilde{\nabla}(\tilde{\nabla}^2\phi)\times\tilde{\nabla}\phi, \tag{16}$$

where

$$\mathrm{Ca}^{-1}=\frac{a^2}{D}\frac{\rho}{\eta}\frac{RT}{M_W}. \tag{17}$$

Note that, according to the mean-field approximation, near the critical point $D=D_0\sqrt{\Psi-2}$, so that, as expected, both the diffusivity and the capillary number vanish at the critical point. This should be kept in mind in the dimensional analysis below, although it does not have any direct relevance to our results, as here we assume that temperature is constant and not too close to the critical point.

The coefficient Ca in Eq. (17) can be interpreted as the capillary number [9], considering that, when the system is composed of patches of almost constant compositions ϕ and $\phi+\Delta\phi$, separated by sharp interfaces, the characteristic length a is proportional to the surface tension σ [cf. Eq. (9)]. In this case, $\mathrm{Ca}=\eta U/\sigma$, with $U=(\Psi-2)^{3/2}(D/a)$ denoting a characteristic diffusion velocity. The coefficient Ca^{-1} is the ratio between thermal and viscous forces, and can be interpreted as a Peclet number, expressing the ratio between convective and diffusive mass flux, i.e., $\mathrm{Ca}^{-1}=Va/D$. Here, V is a characteristic velocity, which can be estimated through Eqs. (2) and (10) as $V\sim F_\phi a^2/\eta$, where $F_\phi\sim\rho RT/(aM_W)$. A similar, so called ''fluidity'' coefficient was also defined by Tanaka and Araki [17]. For systems with very large viscosity, Ca tends to infinity, so that the model describes the diffusion-driven separation process of polymer melts and alloys [13]. For most liquids during phase separation, however, Ca is very small, with typical values ranging from 10^{-3} to 10^{-5}. Therefore, it appears that diffusion is important only at the very beginning of the separation process, in that it creates a nonuniform concentration field. Then, the concentration-gradients-dependent capillary force induces a convective material flux, which dominates the successive process of mass transport. At no time, however, can the diffusive term in Eq. (15) be neglected, as it stabilizes the interface and saturates the initial exponential growth. In addition, it should be stressed that the stream function ψ depends on high order derivatives of the concentration and therefore it is very sensitive to the concentration profile within the interface.

III. RESULTS

A. Numerical scheme and values of the parameters

The governing equations (15) and (16) are solved on a uniform two-dimensional square grid with constant width $[(x_i,y_j)=(i\Delta x,j\Delta y),\ i=1,N,j=1,N]$ and time discretization $[t=n\Delta t,n=0,1,2,\ldots]$. The physical dimensions of the grid are chosen such that $\Delta x/a,\Delta y/a\approx 0.5-2$, while the time step Δt satisfies $\Delta t/(a^2/D)\approx 0.1-0.001$. The choice of the time step Δt is determined semiempirically in order to maintain the stability of the numerical scheme. Note that the nonlinearity of the equations prevents a rigorous derivation of the stability constraints on Δt, but one can roughly estimate that the size of Δt will scale as $O(\Delta x^4,\Delta y^4)$, which is the order of the highest operator in the discretized system. The space discretization is based on a cell-centered approximation of both the concentration variable ϕ and of the stream function ψ. The spatial derivatives in the right-hand side of Eqs. (15) and (16) are discretized using a straightforward second-order accurate approximation. The time integration from $t^n=n\Delta t$ to $t^{n+1}=(n+1)\Delta t$ is achieved in two steps. First, we compute the stream function ψ by solving the biharmonic equation (16) with the source term evaluated at time $t^n=n\Delta t$. The biharmonic equation is solved using the DBIHAR routine from netlib [18]. Second, Eq. (15) is advanced in time, using the velocity field computed from the updated stream function and a straightforward explicit Eulerian step. This makes the entire scheme $O(\Delta t)$ accurate in time, which is acceptable for our problem, since the size of the time step is kept very small anyway by the stability constraints. The boundary conditions are no-flux for the concentration field and no-slip for the velocity field. The discretization of the derivatives near the boundaries is modified to use only interior points. In general, our results are not very sensitive to the precise treatment of boundary conditions, since the gradients remain close to zero near the boundaries. The background noise is simulated generating a random concentration field of amplitude $\delta\phi=0.01$. The same level of noise was maintained during the whole calculation, by adding it at each time step, and then subtracting it at the next (see [13]). The role of the noise in our simulation is mainly to break numerical symmetry and trigger the formation of drops, but it becomes quickly irrelevant once the system reaches the nonlinear regime. For this reason, the detailed form of the noise is not expected to affect the results. In most of our simulations we used $\Psi=2.1$, because this is the Margules parameter of the water-acetonitrile-toluene mixture at 20 °C that was used in a parallel experimental study [1]. However, simulations with different values of Ψ were also performed, obtaining very similar results. When $\Psi=2.1$, at equilibrium the two phases have compositions $(\phi_d)_{\mathrm{eq}}=0.685$ and $(\phi_c)_{\mathrm{eq}}=0.315$. In addition, we used a capillary number $\mathrm{Ca}=10^{-3}-10^{-4}$, which is typical for low-viscosity fluid mixtures.

B. Motion of a single drop in a concentration gradient

Consider an isothermal system composed of a drop with radius R and concentration ϕ_d, surrounded by a continuum phase with concentration $\phi_c=1-\phi_d$ and an imposed initial concentration gradient $\nabla\phi_c$. Since the width of the interface

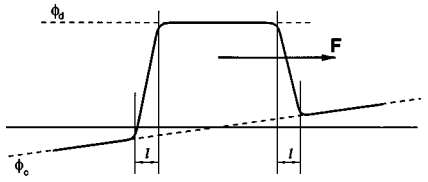

FIG. 1. Isolated drop in a concentration field.

$\ell \approx a/\sqrt{\Psi-2}$ is constant, while the concentration drop across the interface, $\Delta\phi=\phi_d-\phi_c$, is larger on one side of the drop than on the other (see Fig. 1), a surface energy difference between the front and the back of the drop will result [cf. Eq. (8)]. This surface energy gradient will induce a Marangoni force, which, in turn, leads to the motion of the drop. Concomitantly, the system is phase separating, with the concentration of the drop and that of the continuum phase tending to their equilibrium values $(\phi_c)_{\rm eq}$ and $(\phi_d)_{\rm eq}$, respectively. Assuming that the mean particle velocity V is much larger than the typical growth rate of the drop, dR/dt, as it phase separates, the concentration around the drop can be considered approximately equal to its unperturbed value (i.e., it varies linearly with position). Therefore, the energy integrated over the surface of the drop (in 3D) is equal to $E=4\pi R^2\sigma$, where σ is the surface tension evaluated at the drop center. Consequently, imposing that the driving force $\mathbf{F}=\nabla E=4\pi R^2\nabla\sigma$ is equal to the drag force $\mathbf{F}=-5\pi\eta R\mathbf{V}$, with $\mathbf{V}$ denoting the constant translational velocity, and where we have assumed that the drop and the surrounding liquid have the same viscosity η, we obtain

$$\mathbf{V}=-\frac{4R}{5\eta}\nabla\sigma=-\frac{4}{5}\sqrt{\Psi-2}(\Delta\phi)^2{\rm Ca}^{-1}\left(\frac{D}{a}\right)R\frac{\nabla\sigma}{\sigma}. \tag{18}$$

Here ${\rm Ca}=(M_W/\rho RT)(\eta D/a^2)$ is the capillary number defined in Eq. (17), and the surface tension σ is given by Eq. (8), with $(\Delta\phi)$ denoting the mean concentration drop across the interface. Finally, using again Eq. (8), we find that $\nabla\sigma/\sigma=-4\nabla\phi_c/(\Delta\phi)$, and considering that $(\Delta\phi)\sim\sqrt{\Psi-2}$, we obtain

$$\mathbf{V}=K\,{\rm Ca}^{-1}\left(\frac{D}{a}\right)R\nabla\phi_c, \tag{19}$$

with $K\sim(\Psi-2)$.

The analysis presented above is valid only when $V\gg dR/dt$, where the growth rate can be estimated as $dR/dt\sim(\Psi-2)^2(D/a)$ [cf. Eq. (21)]. Therefore the condition of validity of this analysis is that the following inequality be satisfied:

$$\frac{{\rm Ca}(\Psi-2)}{|R\nabla\phi_c|}\ll 1. \tag{20}$$

A similar treatment was presented by Karpov and Oxtoby [11]. Although this model is valid for 3D systems and uses rough approximations for both Marangoni's and drag forces, it describes qualitatively the velocity dependence on the concentration gradient and the capillary number. The dependence on the drop size is obviously a strong function of the dimensionality of the problem, as in 2D Stokes' paradox prevents us from evaluating the drag of the drop (in fact, it should be infinite).

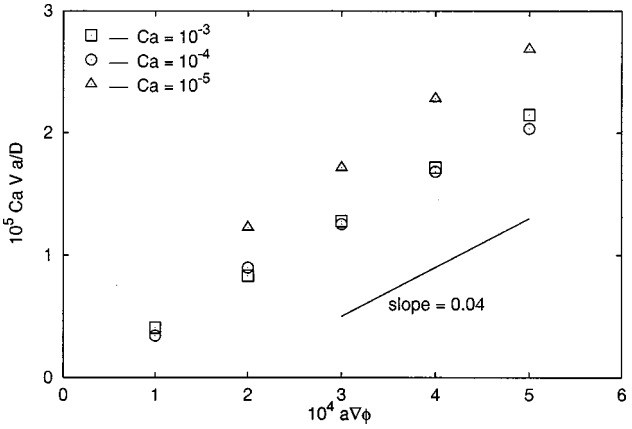

FIG. 2. Velocity $\mathbf{V}$ of a drop with initial radius $R_0=10a$ as a function of the unperturbed concentration gradient $\nabla\phi_c$ of the continuum phase.

The problem of this section is somewhat similar to that studied by Subramanian [19], who generalized Young, Goldstein, and Block's [20] results on thermocapillary motion to the case of a single drop, immersed in an immiscible background phase, while a solute, miscible in both phases, is diffusing within the whole domain, i.e., in and out of the drop. Assuming that the surface tension σ depends on the local solute concentration c, an imposed concentration gradient of the solute, $(\nabla c)_\infty$, would generate a Marangoni force, inducing the motion of the drop. Not surprisingly, in the dilute limit, $c\ll 1$, as the solute concentration c satisfies the heat equation, the migration velocity of the drop $\mathbf{V}$ is given by an expression similar to Young, Goldstein, and Block's [20] thermocapillary velocity, i.e. [19], $\mathbf{V}\sim(\partial\sigma/\partial c)\,\eta^{-1}R(\nabla c)_\infty$. Clearly, apart from a numerical coefficient, this formula is equivalent to Eq. (19), showing that the migration velocity is proportional to the concentration gradient and to the drop size, and is inversely proportional to the viscosity of the fluids (which means that it is inversely proportional to the capillary number Ca).

In our simulations, the drop had an initial radius $R_0=10a$, with average concentration $\phi_d=0.55$ and was im-

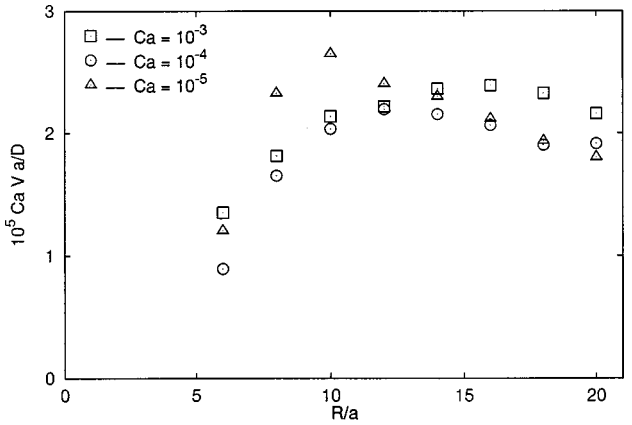

FIG. 3. Velocity $\mathbf{V}$ of a drop with initial radius $R_0=10a$ as a function of its radius, for a given concentration gradient $|\nabla\phi_c|=5\times10^{-4}a^{-1}$ of the continuum phase.

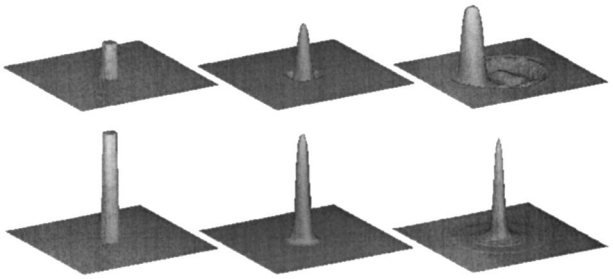

FIG. 4. Concentration field of a drop with initial radius $R_0 = 10a$ and capillary number $\mathrm{Ca} = 10^{-4}$, immersed in a continuum phase with initial concentration depth $(\Delta\phi)_0 = 0.035$ (top) and $(\Delta\phi)_0 = -0.015$ (bottom) at three successive instants of time, $t = 0$, 200, and $2000a^2/D$. The two-dimensional square grid has size $200a$.

mersed in a concentration gradient of the continuum phase, $|\nabla\phi_c| = 10^{-4} - 10^{-3}a^{-1}$. As expected, since the inequality (20) is satisfied, we observed that the drop moves straight in the direction of $\nabla\phi_c$, with a speed that is proportional to $|\nabla\phi_c|$ and inversely proportional to the capillary number Ca (see Fig. 2), in agreement with Eq. (19). However, comparing the results of Fig. 2 with the predictions of Eq. (19), we see that, instead of a slope $K \sim (\Psi - 2) \sim 10^{-1}$, we obtain $K \approx 0.04(R/a) \sim 4 \times 10^{-3}$. As already mentioned, the smaller than expected absolute value of the velocity is probably related to the very large drag experienced by the 2D drop. The dependence of the translational velocity on the drop size is also more complex than the simple linear relation predicted by Eq. (19); in fact, as shown in Fig. 3, it appears that $\mathbf{V}$ depends linearly on R only for small R's, or equivalently, for small concentration gradients, while for larger R's the velocity of the drop evens out, reaching a plateau. Similar results were obtained by Jasnow and Viñals [9], who applied the model H to study the thermocapillary migration of drops.

C. Motion of a single drop in a uniform concentration field

Consider an isolated drop with uniform initial concentration $(\phi_d)_0$ immersed in a concentration field with uniform initial concentration $(\phi_c)_0 = 1 - (\phi_d)_0$. Since the concentration of the drop and that of the continuum phase tend to their respective equilibrium values, the drop will absorb (or desorb) material from (or to) the background field. In doing so, the concentration profile around the drop will become nonuniform, thereby inducing a body force $\mathbf{F}_\phi$ which may lead to the motion of the drop. As we see in Fig. 4, the movement of the drop depends on whether the initial concentration depth $(\Delta\phi)_0 = (\phi_c)_0 - (\phi_c)_{\mathrm{eq}}$ is positive or negative. In the first case, the drop absorbs material from the surrounding continuum phase, digging a ditch all around its perimeter and inducing the capillary driving force $\mathbf{F}_\phi$ which then leads to the motion of the drop. So, the drop motion is self-sustained: each drop generates a change of the surrounding continuum phase, which in turn induces a force which moves the drop. On the other hand, when $(\Delta\phi)_0 < 0$, the drop diffuses out and eventually disappears, without moving. This is due to the fact that the concentration profile in the case $(\Delta\phi)_0 < 0$ is stable, while when $(\Delta\phi)_0 > 0$ it is unstable, as the analysis appearing in a forthcoming article will show. Clearly, when $(\Delta\phi)_0 = 0$, the drop is at equilibrium with the background field and does neither move nor change its size.

While a drop immersed in a concentration gradient moves even when its size remains constant, the motion of a drop immersed in a uniform concentration field with $(\Delta\phi)_0 > 0$ is

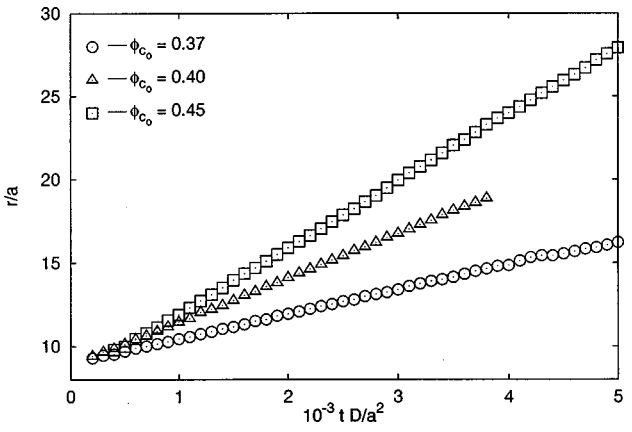

FIG. 5. Radius of a phase-separating drop as a function of time. The drop, with initial radius $R_0 = 9.5a$, is immersed in a uniform concentration field with initial composition $(\phi_c)_0 = 0.35$, 0.40, and 0.45, and with equilibrium composition $(\phi_c)_{\mathrm{eq}} = 0.315$.

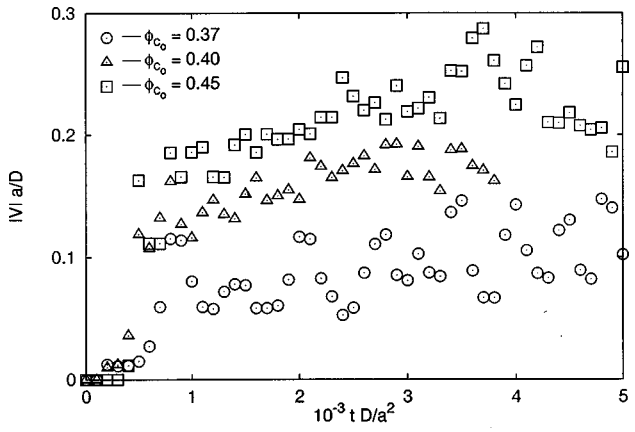

FIG. 6. Instantaneous velocity $|V|$ of a phase-separating drop immersed in a uniform concentration field with initial composition $(\phi_c)_0 = 0.35$, 0.40, and 0.45, and with equilibrium composition $(\phi_c)_{\mathrm{eq}} = 0.315$.

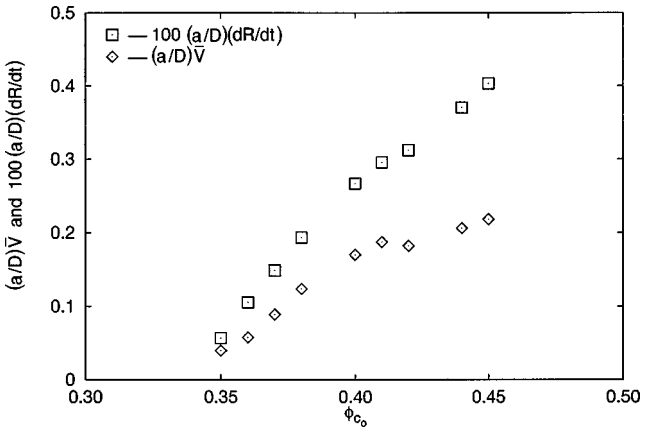

FIG. 7. Mean velocity, $\bar{V}$, and growth rate dR/dt, as functions of the initial concentration depth $(\Delta\phi)_0$.

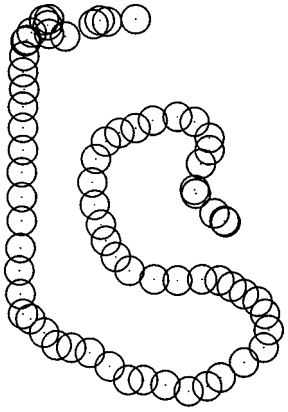

FIG. 8. Trajectory of a drop with initial radius $R_0=9.5a$, immersed in a uniform continuum phase with initial composition $(\phi_c)_0=0.45$ and capillary number $\mathrm{Ca}=10^{-4}$. The position of the drop is shown at each time interval $\Delta t=100a^2/D$; and the size of square grid is $400a$.

intrinsically connected to its changing size, i.e., if the drop does not absorb material from the background field, it will not move. In Fig. 5 the drop radius is plotted as a function of time, showing that the growth rate dR/dt is constant, even in the case $(\Delta\phi)_0=0.315$, when the drop radius increases four times during the time interval considered. This has to be expected, considering that $dR/dt=|\mathbf{j}|/\rho$, where $\mathbf{j}$ is the mass flux at the interface, which, far from equilibrium, can be estimated as $|\mathbf{j}|\sim\rho(\Delta\phi)[2\phi(1-\phi)\Psi-1](a/\ell)(D/a)$, with $\ell\sim a/\sqrt{\Psi-2}$ denoting the characteristic thickness of the interface [13]. Therefore, assuming that the drop is near local equilibrium, and considering that $(\Delta\phi)_{\mathrm{eq}}\sim\sqrt{\Psi-2}$, we obtain

$$\frac{dR}{dt}\sim\beta\frac{D}{a}, \tag{21}$$

where $\beta\sim(\Psi-2)^2$. In our case, with $\Psi=2.1$, we can estimate $\beta\sim10^{-2}D/a$, in agreement with the results of our simulations (see Fig. 4), and confirming that the growth rate is independent of the drop radius. Although the local equilibrium assumption gives the correct estimate (21), it is by no means accurate [17], and in fact it cannot account for the dependence of the drop growth rate on $(\Delta\phi)_0$. Note that, using the values $a\sim10^{-5}$ cm, $D\sim10^{-5}$ cm^2/s and $\Psi=2.1$, which are characteristic of the liquid mixture used in Ref. [1], we would predict $dR/dt\sim100$ μm/s, in good agreement with our experimental observations.

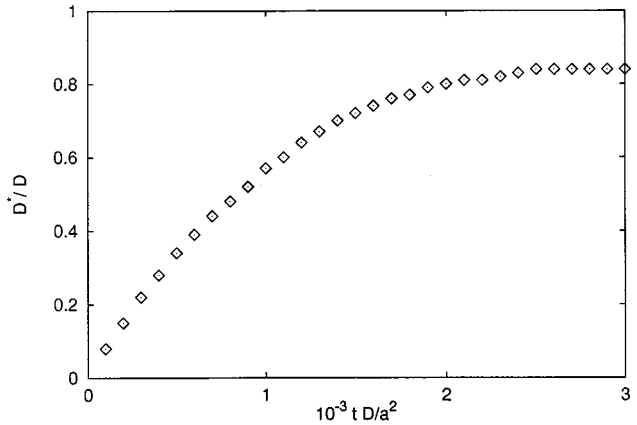

FIG. 9. Effective diffusivity D^* of a drop with initial radius $R_0=9.5a$, immersed in a continuum phase with initial composition $(\phi_c)_0=0.40$ and capillary number $\mathrm{Ca}=10^{-4}$.

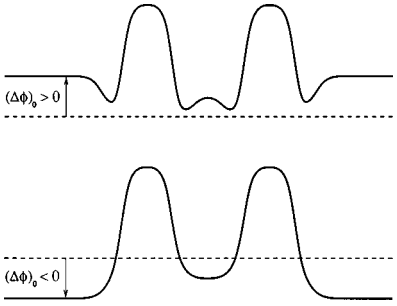

FIG. 10. Sketches of the concentration profiles of two phase-separating drops when $(\Delta\phi)_0>0$ (top), and $(\Delta\phi)_0<0$ (bottom).

In Fig. 6, the instantaneous velocity of the drop, $|V|$, with $(\Delta\phi)_0>0$, is plotted as a function of time, showing that it strongly fluctuates around its mean value $\overline{V}$. In turn, the latter depends on the driving force that is proportional to the concentration depth $(\Delta\phi)_0$ of the ditch that the drop ''digs'' all over its perimeter (see Fig. 4). The dependence of $\overline{V}$ and dR/dt on $(\Delta\phi)_0$ is represented in Fig. 7, revealing that both quantities do not depend on R, while they increase with $(\Delta\phi)_0$, vanishing when $(\Delta\phi)_0\approx0.01$. This latter result

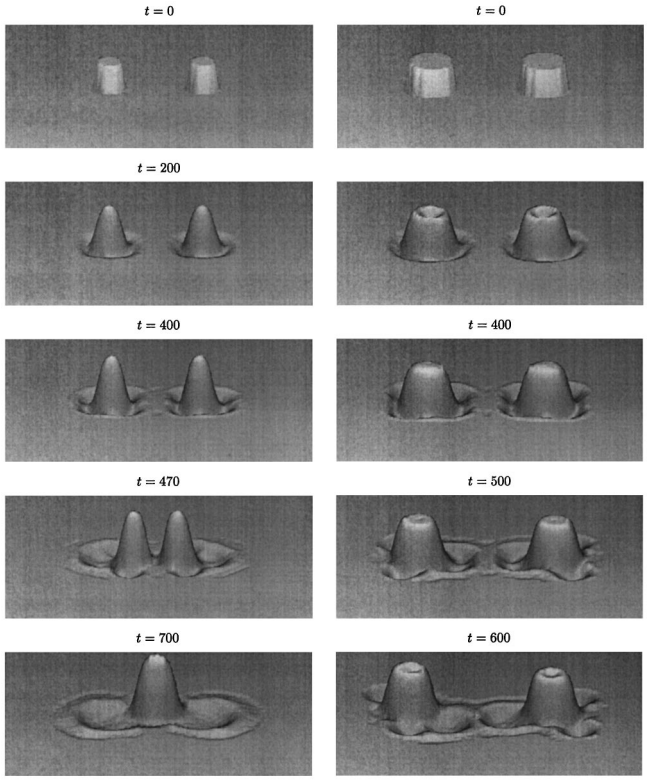

FIG. 11. Evolution of the concentration field of two identical drops with initial radii $10a$ (left) and $16a$ (right), immersed in a continuum phase with $(\Delta\phi)_0=0.135$. The two-dimensional square grid has size $200a$; and time is expressed in a^2/D units.

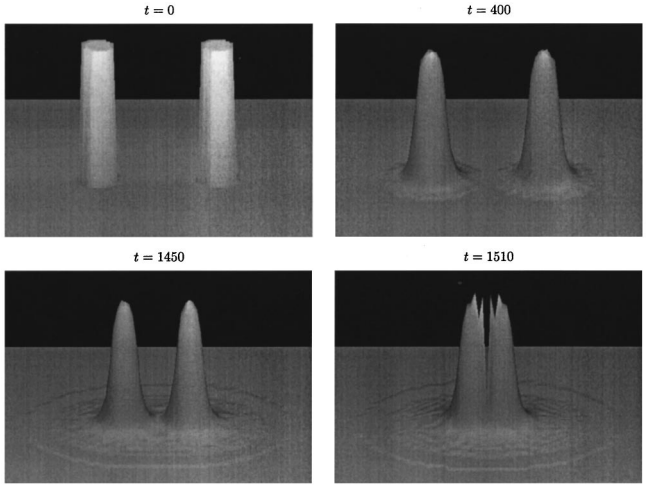

FIG. 12. Evolution of the concentration field of two identical drops with initial radius $10a$, immersed in a continuum phase with $(\Delta\phi)_0 = -0.015$. The two-dimensional square grid has size $200a$; and time is expressed in a^2/D units.

seems to indicate that when the initial concentration depth $(\Delta\phi)_0$ is very small, the system finds itself in a metastable state, from which it can evolve only in the presence of a finite disturbance. Note that for the liquid mixture of Ref. [1] we would predict $\overline{V} \sim 1$ mm/s, in good agreement with our experimental observations.

Following the motion of the drop, as in Fig. 8, we see that its motion looks random. In fact, denoting by $\mathbf{r}(t)$ the position of the center of the drop at time t, with $\mathbf{r}(0)=0$, we can define the effective diffusivity D^* as

$$D^* = \frac{\langle [r(t)]^2 \rangle}{4t}. \tag{22}$$

In Fig. 9 the effective diffusivity is plotted, showing that it does tend to an $O(D)$ constant value for long times. The fact that a drop has a diffusivity which is of the same magnitude as that of its molecules is typical of critical phenomena, where correlation lengths are very large, but it is extremely unusual in continuum mechanics.

D. Motion of two drops in a uniform concentration field

In the simulations of Fig. 4 we saw that drops modify their surrounding continuum phase and then they may move accordingly, driven by a capillary force which is proportional to the concentration gradient. Therefore, when two drops are close enough that each modifies the concentration distribution of the continuum phase surrounding the other, we expect that the net effect will be a mutual attractive force. In other words, as an *A*-rich drop travels towards regions with higher concentration of *A*, growing in size and leaving behind tails of purified *B*-rich fluid, it will influence the motion of another *A*-rich drop nearby. In general, this attractive force can be seen as an attempt of the system to minimize its interfacial area and, therefore, its free energy, as described by Tanaka [21].

In our simulation, we assume that the drops start interacting with each other before they die out. That occurs, provided that the ratio between the drops' initial mutual distance and their radius is larger than the ratio between their typical speed and shrinking rate. In turn, the typical drop speed depends on the concentration distribution around the dissolving drop, and therefore it is a function of $(\Delta\phi)_0$.

Similarly to the single drop case, our simulations revealed that the behavior of the system depends on whether $(\Delta\phi)_0$ is positive or negative. In fact, as the two drops start to move towards each other, when $(\Delta\phi)_0 > 0$ the concentration profile tends to form a concentration barrier, screening their mutual attraction, while when $(\Delta\phi)_0 < 0$ the mutual attractive force is unchallenged (see Fig. 10). Consequently, when $(\Delta\phi)_0 > 0$, the two drops may or may not coalesce as they approach each other, while when $(\Delta\phi)_0 < 0$ they always end up coalescing (provided they do not die out sooner), as shown in Figs. 11 and 12, respectively. Note that despite few bursts expressing singular behavior, our computer model seems adequate in describing the process of two drops merging into one.

ACKNOWLEDGMENT

During this work, N.V. and R.M. were supported in part by the National Science Foundation under Grant No. CTS-9634324.

[1] R. Gupta, R. Mauri, and R. Shinnar, Ind. Eng. Chem. Res. **35**, 2360 (1996); *ibid.* **38**, 2418 (1999).
[2] N.C. Wong and C. Knobler, J. Chem. Phys. **69**, 725 (1978); Phys. Rev. A **24**, 3205 (1981); E. Siebert and C. Knobler, Phys. Rev. Lett. **54**, 819 (1985).
[3] Y.C. Chou and W.I. Goldburg, Phys. Rev. A **20**, 2015 (1979); A.J. Schwartz, J.S. Huang, and W.I. Goldburg, J. Chem. Phys. **62**, 1847 (1975); **63**, 599 (1975).
[4] P. Guenoun, R. Gastaud, F. Perrot, and D. Beysens, Phys. Rev. A **36**, 4876 (1987); P. Guenoun, D. Beysens, and M. Robert, Phys. Rev. Lett. **65**, 2406 (1990); D. Beysens, P. Guenoun, P. Sibille, and A. Kumar, Phys. Rev. E **50**, 1299 (1994).
[5] E. Siggia, Phys. Rev. A **20**, 595 (1979).
[6] Reviews on spinodal decomposition can be found in J.S. Langer, in *Systems Far from Equilibrium*, edited by L. Garrido, Lecture Notes in Physics Vol. 132 (Springer-Verlag, Berlin, 1980); J.D. Gunton, M. San Miguel, and P.S. Sahni, in *Phase Transition and Critical Phenomena*, Vol. 8, edited by C. Domb and J.L. Lebowitz, (Academic Press, London, 1983), Vol. 8.
[7] K. Kawasaki, Ann. Phys. (N.Y.) **61**, 1 (1970).
[8] P.C. Hohenberg and B.I. Halperin, Rev. Mod. Phys. **49**, 435 (1977).
[9] D. Jasnow and J. Viñals, Phys. Fluids **8**, 660 (1996).
[10] V.G. Karpov, Phys. Rev. Lett. **75**, 2702 (1995).
[11] V.G. Karpov and D.W. Oxtoby, Phys. Rev. E **55**, 7253 (1997).
[12] L. Landau and L. Lifshitz, *Fluid Mechanics* (Pergamon, New York, 1953).
[13] R. Mauri, R. Shinnar, and G. Triantafyllou, Phys. Rev. E **53**,

2613 (1996); N. Vladimirova, A. Malagoli, and R. Mauri, *ibid.* **58**, 7691 (1998).
[14] J.W. Cahn and J.E. Hilliard, J. Chem. Phys. **28**, 258 (1958); **31**, 688 (1959); J.W. Cahn, *ibid.* **30**, 1121 (1959); Acta Metall. **9**, 795 (1961).
[15] J.D. van der Waals, Z. Phys. Chem., Stoechiom. Verwandtschaftsl. **13**, 657 (1894); J. Stat. Phys. **20**, 200 (1979).
[16] J.E. Farrell and O.T. Valls, Phys. Rev. B **40**, 7027 (1989); **42**, 2353 (1990); **43**, 630 (1991).
[17] H. Tanaka and T. Araki, Phys. Rev. Lett. **81**, 389 (1998).
[18] P. Bjorstad, Ph.D. dissertation, Stanford University, 1980.
[19] R.S. Subramanian, J. Fluid Mech. **153**, 389 (1985).
[20] N.O. Young, J.S. Goldstein, and M.J. Block, J. Fluid Mech. **6**, 350 (1959).
[21] H. Tanaka, Phys. Rev. E **51**, 1313 (1995); J. Chem. Phys. **105**, 10 099 (1996); **107**, 3734 (1997).